FINAL
CONTRACT REPORT

IMPLEMENTATION AND NON-DESTRUCTIVE EVALUATION OF COMPOSITE STRUCTURAL SHAPES IN THE TOM'S CREEK BRIDGE

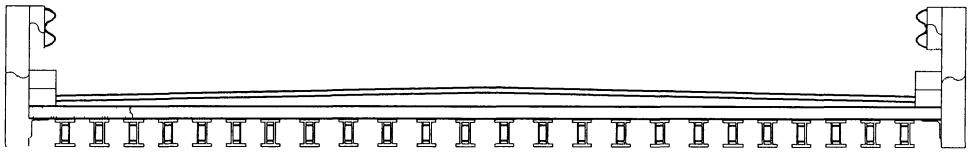

M. D. Hayes, J. Haramis, J. J. Lesko,
T. E. Cousins, J. C. Duke, R. E. Weyers

Department of Engineering Science and Mechanics
and Via Department of Civil
and Environmental Engineering
Virginia Polytechnic Institute and State University

VIRGINIA TRANSPORTATION RESEARCH COUNCIL

Standard Title Page - Report on Federally Funded Project

1. Report No. FHWA/VTRC 00-CR7	2. Government Accession No.	3. Recipient's Catalog No.
4. Title and Subtitle Implementation and Non-Destructive Evaluation of Composite Structural Shapes in the Tom's Creek Bridge		5. Report Date May 2000 6. Performing Organization Code
7. Author(s) M.D. Hayes, J. Haramis, J.J. Lesko, T.E. Cousins, J.C.Duke, R.E. Weyers		8. Performing Organization Report No. VTRC 00-CR7
9. Performing Organization and Address Virginia Transportation Research Council 530 Edgemont Road Charlottesville, VA 22903		10. Work Unit No. (TRAIS) 11. Contract or Grant No. 5105-020 and 1432-020
12. Sponsoring Agencies' Name and Address Virginia Department of Transportation 1401 E. Broad Street Richmond, VA 23219 FHWA P.O. Box 10249 Richmond, VA 23240		13. Type of Report and Period Covered FINAL November 1997 – May 2000 14. Sponsoring Agency Code
15. Supplementary Notes		

16. Abstract

A bridge rehabilitation utilizing a hybrid fiber reinforced polymeric composite has been completed in Blacksburg, Virginia. This project involved replacing the superstructure in the Tom's Creek Bridge, a rural short-span traffic bridge with a timber deck and corroded steel girders, with a glue-laminated timber deck on composite girders. In order to verify the bridge design and to address construction issues prior to the rehabilitation, a full-scale mock-up of the bridge was built and tested in the laboratory. This set-up utilized the actual composite beams, glue-laminated timber deck panels, and geometry to be implemented in the rehabilitation. After the rehabilitation was completed, the bridge was field tested under a known truckload. Both tests examined service load deflections, girder strains, load distribution, the degree of composite action, inter-panel deck deflections, and impact factor. The field test results indicate a service load deflection of L/400 under moving loads and a factor of safety of over 7 using the projected A-allowable for beam flexural strength. The data from the field test serves as a baseline reference for future field durability assessments as part of a long-term performance and durability study.

17 Key Words	18. Distribution Statement
Composite materials, bridge rehabilitation, field testing, non-destructive testing	No restrictions. This document is available to the public through NTIS, Springfield, VA 22161.

19. Security Classif. (of this report)	20. Security Classif. (of this page)	21. No. of Pages	22. Price
Unclassified	Unclassified	31	

Form DOT F 1700.7 (8-72) Reproduction of completed page authorized

FINAL CONTRACT REPORT

IMPLEMENTATION AND NON-DESTRUCTIVE EVALUATION OF COMPOSITE STRUCTURAL SHAPES IN THE TOM'S CREEK BRIDGE

M.D. Hayes[1], J. Haramis[2], J.J. Lesko[1], T.E. Cousins[2], J.C. Duke[1], R.E. Weyers[2]

[1]Department of Engineering Science and Mechanics
[2]Via Department of Civil and Environmental Engineering
Virginia Polytechnic Institute and State University
Blacksburg, Virginia 24061

Project Monitor
Dr. Jose Gomez, Virginia Transportation Research Council

Contract Research Supported by
Virginia Transportation Research Council

Virginia Transportation Research Council
(A Cooperative Organization Sponsored Jointly by the
Virginia Department of Transportation and
the University of Virginia)

Charlottesville, Virginia Tech

May 2000
VTRC 00-CR7

NOTICE

The project that is the subject of this report was done under contract for the Virginia Department of Transportation, Virginia Transportation Research Council. The opinions and conclusions expressed or implied are those of the contractors, and, although they have been accepted as appropriate by the project monitors, they are not necessarily those of the Virginia Transportation Research Council or the Virginia Department of Transportation.

Each contract report is peer reviewed and accepted for publication by Research Council staff with expertise in related technical areas. Final editing and proofreading of the report are performed by the contractor.

ABSTRACT

A bridge rehabilitation utilizing a hybrid fiber reinforced polymeric composite has been completed in Blacksburg, Virginia. This project involved replacing the superstructure in the Tom's Creek Bridge, a rural short-span traffic bridge with a timber deck and corroded steel girders, with a glue-laminated timber deck on composite girders. In order to verify the bridge design and to address construction issues prior to the rehabilitation, a full-scale mock-up of the bridge was built and tested in the laboratory. This set-up utilized the actual composite beams, glue-laminated timber deck panels, and geometry to be implemented in the rehabilitation. After the rehabilitation was completed, the bridge was field tested under a known truckload. Both tests examined service load deflections, girder strains, load distribution, the degree of composite action, inter-panel deck deflections, and impact factor. The field test results indicate a service load deflection of L/400 under moving loads and a factor of safety of over 7 using the projected A-allowable for beam flexural strength. The data from the field test serves as a baseline reference for future field durability assessments as part of a long-term performance and durability study.

IMPLEMENTATION AND NON-DESTRUCTIVE EVALUATION OF COMPOSITE STRUCTURAL SHAPES IN THE TOM'S CREEK BRIDGE

M. D. Hayes
Department of Engineering Science and Mechanics
Virginia Polytechnic Institute and State University

J. Haramis
Department of Engineering Science and Mechanics
Virginia Polytechnic Institute and State University

J. J. Lesko
Department of Engineering Science and Mechanics
Virginia Polytechnic Institute and State University

T. E. Cousins
Department of Civil Engineering
Virginia Polytechnic Institute and State University

J. C. Duke
Department of Engineering Science and Mechanics
Virginia Polytechnic Institute and State University

R. E. Weyers
Department of Civil Engineering
Virginia Polytechnic Institute and State University

INTRODUCTION

Fiber reinforced polymeric (FRP) composites have great potential for use in infrastructure and other civil engineering applications. Composites may offer a number of advantages over traditional materials, including environmental durability and ease of construction due to high specific strength. However, a number of technical issues remain and must be addressed before the civil engineering community can develop confidence in structural design with composite members. These issues include low stiffness, confirmation of improved durability, cost, variability, and connection details. The low modulus of FRP composites often results in structures that deflect more than their steel and reinforced concrete counterparts. Excessive deflections can damage the deck overlay system, limiting its serviceability and requiring more frequent maintenance.

Enviro-mechanical durability is often cited as a key advantage of FRP composite materials over steel designs; composites do not exhibit corrosion, i.e. a material state change. However, polymer resins and glass fibers do experience state changes through more complex mechanisms. Polymer stiffness, toughness and strength can be reduced when exposed to moisture, UV, and temperature. Glass fibers experience degradation in the presence of moisture and low pH as a result of a stress corrosion mechanism. The effects of these processes on global laminate and structural properties (stiffness, strength, and life) are not yet fully understood. Degradation kinetics and the synergistic interactions of these mechanisms are even less understood.

If composites prove more durable in infrastructure environments, they must still compete with conventional materials on first cost. At this point, however, the raw material costs of composites is much higher than steel, concrete, and timber resulting in a significantly higher first cost of composite components. The competitiveness of composites in bridge structures most likely falls in the potential for lower life cycle and/or installation costs.

The complexity of composite materials in terms of mechanics, chemistry, and life prediction can also be a deterrent to the use of composites in bridges by the civil engineer. Composites, unlike metals, do not conform to a linear cumulative damage approach to describing remaining life; composite damage is dependent on the path by which it has reached its present damage state. The variability in constituent materials, fiber architecture, and manufacturing processes employed in fabricating composite members also makes generalizations about performance difficult. The orthotropy of composite plates and the tendency to delaminate at free edges also require special attention when considering performance.

The authors believe that establishing field test sites to assess the structural behavior and durability of composite material systems in actual service environments and loading scenarios is key in developing confidence in design with FRP composites within the civil engineering community. By working with state departments of transportation, local cities and towns, manufacturers of composite systems, and research groups, the community can develop experience in choosing specific composite systems for certain applications and in utilizing those materials in efficient, cost-effective, and safe applications. These interactions are crucial to the development of standards and practices for the use of composite material systems in civil structures as well as a transfer of technology.

Recently, a number of small vehicular traffic bridges have been constructed using composite members (reviewed in Hayes 1998). These projects demonstrate how composites might be implemented in future bridge construction or rehabilitation. Such experimental efforts also serve as test cases for experimental composite systems, and an opportunity to assess their enviro-mechanical durability through a monitoring program.

The Tom's Creek Bridge in Blacksburg, VA is an example of one such experimental test site for composite bridge structures and materials. This paper reports the pertinent findings from the laboratory testing, design, construction, and field testing of the Tom's Creek Bridge. This bridge rehabilitation utilizes a hybrid fiber reinforced polymeric composite pultruded cross section as the bridge girder. The rehabilitation effort involved replacing the superstructure of the Tom's Creek Bridge, a rural short-span traffic bridge two miles from the Virginia Tech campus.

Beyond the rehabilitation effort, further work is underway to study the beam's durability under monitored enviro-mechanical service conditions.

Tom's Creek Bridge Rehabilitation Project

The Tom's Creek Bridge rehabilitation presents an opportunity for a field site investigation. This program was initiated in an effort to rehabilitate the Tom's Creek Bridge in Blacksburg, Virginia. Through the partnership of Virginia Tech, the Virginia Department of Transportation (VDOT), the Virginia Transportation Research Council (VTRC), the Town of Blacksburg, and Strongwell Corporation (formerly Morrison Molded Fiber Glass), rehabilitation of the Tom's Creek Bridge superstructure was completed in June of 1997 using a new hybrid composite beam. The original bridge structure, a 6.1 m long and 7.32 m wide single-span bridge, was constructed of twelve steel W10x21 stringers spacing 6100 mm apart, supporting a timber deck, roughly 95 mm in depth, including a 75 mm thick asphalt overlay. This superstructure rests on concrete abutments, skewed 12.5° from normal. The bridge was originally built in 1932 and later rehabilitated in 1964. The designed load capacity was 178 kN.

Inspection of the bridge in January 1990 revealed significant corrosion of the steel stringers, which was attributed to the humid environment and occasional flooding of the Tom's Creek. The loss in stringer section prompted the Town of Blacksburg to reduce the posted load capacity to 89 kN. The town needed a repair option to extend the life of the bridge another 10-15 years. The collaboration of academia, industry, and government resulted in a plan to replace the 12 steel members with 24 composite box-I or double-web beams, developed and manufactured by Strongwell and Georgia Tech (Strongwell, 1994). The completed bridge is shown in Figure 1. The details of the rehabilitation to the AASHTO HS20-44 standard and the details of the new bridge design are published (Hayes, 1998 & 2000) and are summarized here.

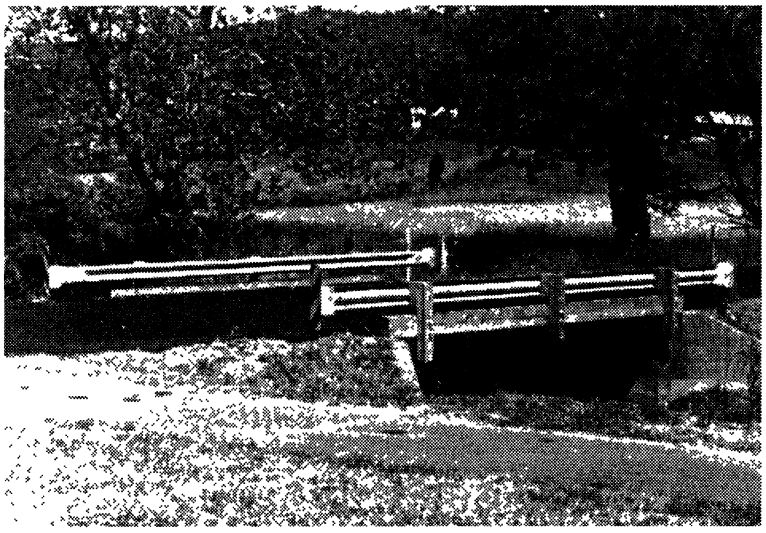

Figure 1. The rehabilitated Tom's Creek Bridge.

Strongwell's Hybrid Composite Box I-Beam

The box-I beam is a 203 mm deep section (see Figure 2) serving as a sub-scale prototype for a 914 mm beam being developed for 10 to 18 m span bridges (Strongwell, 1994). The beam is a pultruded section composed of both E-glass and carbon fiber in a vinyl ester resin. The approximate fiber volume fraction (both glass and carbon) for the structure is 55%. The carbon is located in the flanges to increase the section's bending stiffness. Glass fiber is present in the pultruded structure in the form of primarily stitched angle ply mats, roving and continuous strand mat. Twenty-four of the beams, fabricated during the development process, were available for use in the Tom's Creek Bridge.

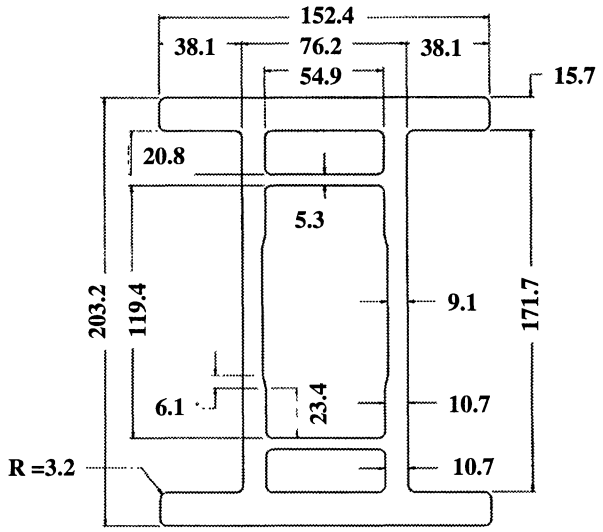

Figure 2. Cross-section of the box I-beam prototype; all dimensions in mm

Rehabilitation Design

In an effort to address the AASHTO HS20-44 design standard the rehabilitation called for a two-for-one replacement of the twelve 254 mm deep steel stringers (W250x33) with the 203 mm deep composite beams (Figure 3). The two-for-one beam replacement was necessary due to the lower section modulus of the prototype composite beam, which is a result of both the lower modulus of the composite material and the shorter height of the composite prototype section. A later scaling analysis of the 203 mm deep section to a 254 mm deep section shows that a one-for-one replacement would have been possible (Hayes, 1998). The composite beams were arranged in the bridge design according to their measured bending modulus (Hayes, 1998). The variation is stiffness (48 MPa using the Hexcel AS-4 fiber as compared to 44 GPa using the Zoltek Panex 33 fiber) resulted from the use of two different carbon fiber types during two separate processing runs. In an effort to improve the load distribution (provide additional stiffness to the edges of the bridge) the stiffer beams were positioned as the outer beams on each side of the bridge, and the spacing between these outer beams was also reduced slightly.

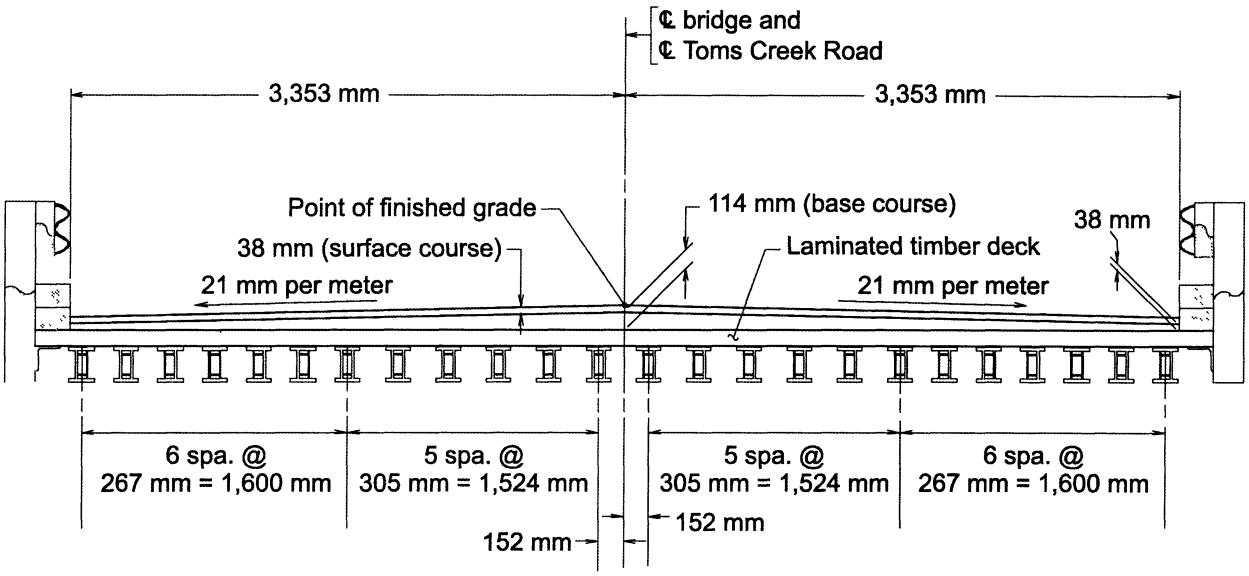

Figure 3. Transverse view from design plans for rehabilitated bridge structure showing placement of composite beams (*Proposed* 1997).

The original timber planking was replaced with a new timber glue laminated system (130 mm thick); the depth of the deck was increased from about 95 mm to 130 mm to accommodate the shallower composite beam. An asphalt overlay, employing a water proofing membrane (Howard, 1997), and a traditional timber and steel guardrail design were utilized. The rail details include 152 mm x 203 mm timber curb rails and posts with steel guard rails mounted to the vertical posts, shown in Figure 4. The posts supporting the guard rail are bolted to the curb rails which are in turn secured to the deck by bolted connections as well.

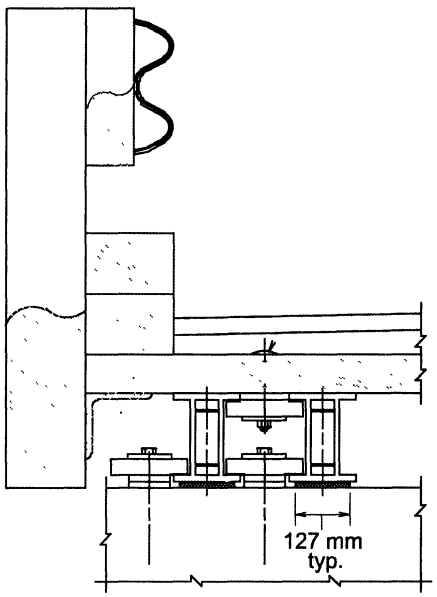

Figure 4. Guard rail/rub rail design (*Proposed* 1997).

PURPOSE AND SCOPE

Although this bridge design is far from efficient (due to the stringer depth), it does represent a unique opportunity to implement composites in a vehicular bridge. It also offers an opportunity to study the structural performance and durability of these materials in a low risk situation. The bridge carries about 1000 vehicles per day; 95% of which are small cars. Furthermore, the bridge is scheduled to be widened in 10-15 years, so the situation offers a unique opportunity to study the composite members at the end of their service life. Continuous monitoring, presently underway, of the service environment and loading experienced by the structure provides a basis for assessing changes in material properties of the composite stringers, and likewise, their effect on the performance of the structure.

METHODS

Experimental Verification of Design

The final design of the composite superstructure for the Tom's Creek Bridge was completed by VDOT with input from Virginia Tech. Specifically, Virginia Tech provided recommendations to VDOT about transverse spacing of the box I-beams, connection details and thickness of the glue-laminated timber deck based on a simple analytical model of the bridge superstructure (Hayes, 1998). Once the design was finalized, it was validated by constructing and testing the full-scale bridge in the laboratory. This mock-up was constructed using the actual composite beams and deck system to be utilized in the rehabilitation and was tested under simulated static axle and wheel loads. The mock-up construction also provided an opportunity to investigate various design details such as connections. Upon completing the rehabilitation in June of 1997, the new structure was field tested. This opportunity again served as an additional validation for the design and model predictions as well as an opportunity to investigate the behavior of the bridge under moving loads. The field testing also helped to identify the effects of beam end conditions and curb stiffening (resulting from curb rail connections to the deck) on the bridge response, since these structures were not employed in the lab testing.

Laboratory Testing of Bridge Girders

The 24 composite box I-beams utilized in the rehabilitation were first tested to roughly two times the predicted maximum service load to determine the stiffness of each beam. Tests of individual beams at a span of 5.74 m have shown an average bending modulus of 44 to 48 GPa (Hayes, 1998). One beam was tested to failure under a four point loading and failed at an applied load of 129 kN, revealing a 152 kN•m moment capacity at a 5.3m span. The shear contribution to deflection is approximately 5% at this span.

Non-Destructive Evaluation

Non-destructive evaluation (NDE) techniques were utilized both during the static testing of the beams (acoustic emission) and in the unstressed state (infrared thermography & acousto-ultrasound) (Duke et al., 1998). These techniques and their application are summarized below.

Infrared Thermography

It was desired to perform a 100% assessment of each of the beams used for this rehabilitation project. Infrared thermography (IRT) was selected for this purpose. This technique is able to map surface temperatures of relatively large areas in short periods of time. It was expected that manufacturing imperfections and other damage (delaminations between plies) would effect heat transfer in the composite beams. Thus, beams were examined by translating them past the IRT camera, located "downstream" from a radiant heat source (a quartz halogen lamp) directed at the surface. This localized heating of the translating beam created the desired thermal gradient to expose potential manufactured or damage defects due to their influence on the heat transfer characteristics associated with that region.

The heat lamp was positioned "upstream" of the infrared camera, determined by trial and error, at a distance to allow for a temperature gradient that would optimally reveal features of the beam structure, as the beams were translated, at a selectable speed, past the heating and detection system. The exterior surfaces of the web sections and the extreme surfaces of the flanges, of each beam were examined separately. Additional beams reserved for mechanical testing were also examined. The IRT images were collected on videotape. Discrimination of defects was accomplished by comparing the image of imperfect regions with images of typically pristine regions.

Acoustic Emission Monitoring

All of the beams installed in the bridge were proof tested, in four-point load bending, to a level anticipated to just slightly exceed the service loads. Acoustic emission (AE) was monitored during each of these tests to provide additional confidence in the condition of the beams. This technique attempts to exploit the fact that most material emits transient mechanical disturbance when microscopic damage mechanisms occur, e.g. matrix cracking, fiber fracture and interfacial failure. The mechanical disturbance is the result of acoustic energy released during the process of failure. The AE sensor, typically placed at the surface of the composite, is then able to detect this energy.

A multi-channel Physical Acoustics Corporation Spartan AT system was used for monitoring the beams during proof-testing. Wide band, differential transducers with preamplifiers integral with the sensor housing (WDI) were attached at locations in close proximity to strain gages bonded to the beams. Because of the high attenuation of the composite materials the source of AE, at large distances from the sensors, are not easily detected. Consequently the sensors are placed in regions of the loaded subject to the highest induced stresses. To establish the sensor locations, prior to performing the proof tests, one beam was loaded and unloaded to successively higher loads until failure occurred. Acoustic emission was monitored throughout this loading procedure using an eight channel monitoring system and all of the parameterized data, including mid point maximum strain were recorded for post-test analysis. The results of this test were used to guide the placement of transducers for the proof testing. Final selection of the AE transducer positions is shown in Figure 5.

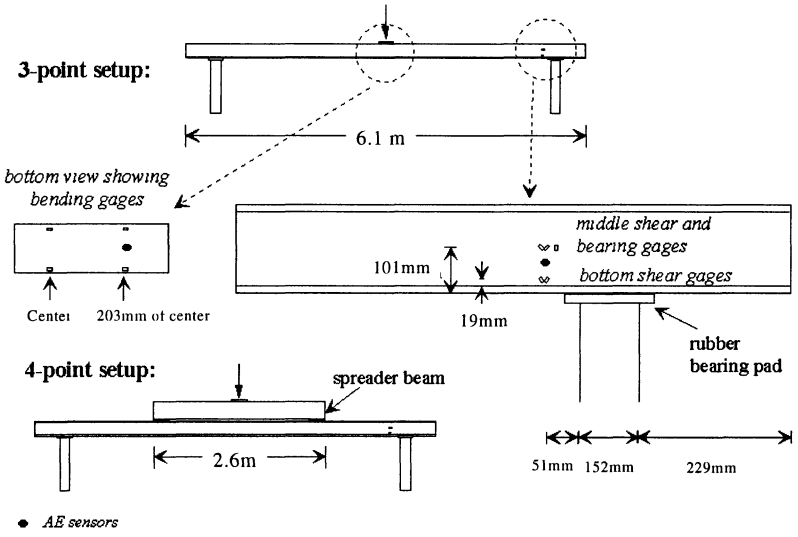

Figure 5. Schematic of proof test configurations used for individual beams indicating the location of AE sensors.

Acousto-Ultrasound Evaluation

The acousto-ultrasonic (AU) method was used in an attempt to assess potential damage in the regions of the beams beneath the load application areas. It was anticipated that such a procedure might be applied to the actual bridge structure to assess the region of interest. The AU method uses the changes detected in an ultrasonics disturbance excited in the component at a location that will allow the disturbance to propagate through the region of interest. The wide band signal received is then analyzed to distinguish changes in frequency content and relative amplitude changes. These spectral characteristics are correlated directly to various damage modes observed in the structure.

Preliminary results for the sensitivity of this approach have been developed during the cyclic loading of a second extra beam. This beam was dynamically loaded at 1 Hz with a sinusoidal wave from at R=0.1 for three million cycles at the maximum design strain level, while AU was

periodically used to assess any changes in the regions of the beam around the loading points. An ultrasonic transducer was employed to induce an ultrasonic disturbance into the component and a second transducer to detect the portion of this disturbance that propagated away from the point of excitation. By positioning the two transducers appropriately it was possible to interrogate the beam with the fiber reinforcement, transverse to the direction of fiber reinforcement, or through the thickness of the flange.

Laboratory Testing of Bridge Superstructure

A full-scale mock-up of the Tom's Creek Bridge structure was constructed in the Civil Engineering Structures and Materials Research Laboratory at Virginia Tech (Figure 6). A steel load frame was built around the bridge structure to mount loading actuators. Steel W27 x 84 foundation beams were used to simulate the existing concrete abutments. These foundation beams were spaced to provide an unsupported span length of 5.3 m and were skewed at an angle of 12.5°. A 6mm thick reinforced rubber pad was laid along the top flange of the foundation beam to simulate the support condition used at the bridge site as well as to prevent abrasion of the composites. The composite beams spanned across the foundation beams with the outer 7 beams of both sides (14 total) spaced 267 mm apart and the middle 10 beams spaced 305 mm apart as constructed in the bridge.

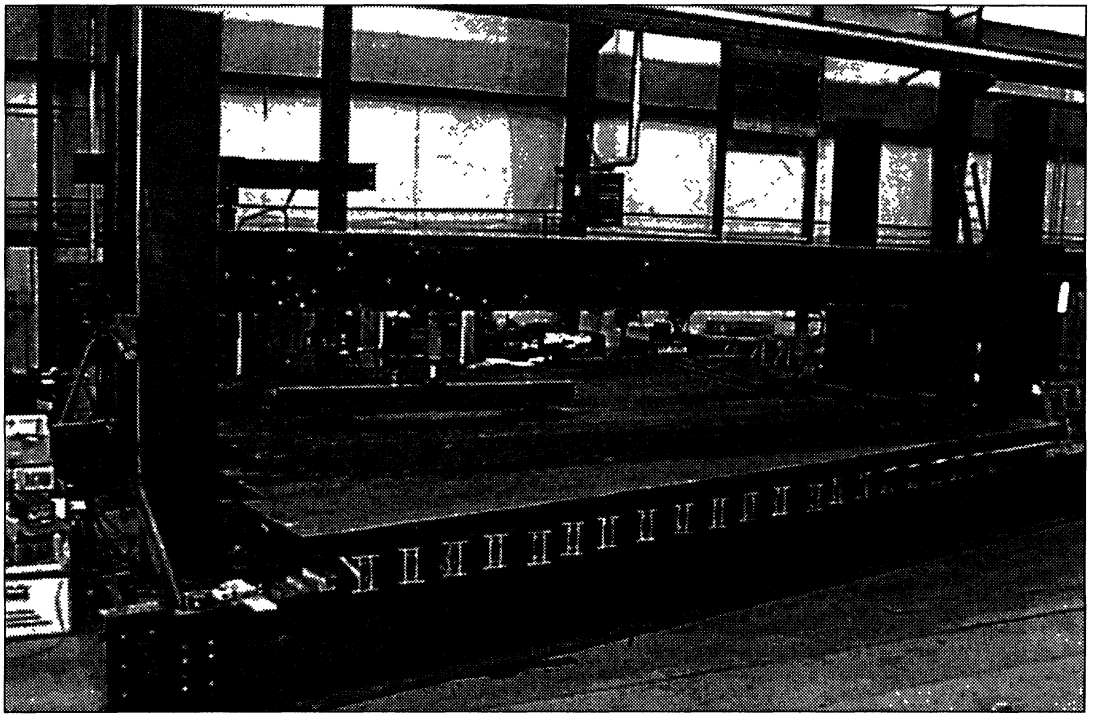

Figure 6. Laboratory mock-up test setup.

The same glue-laminated deck employed in the rehabilitation was also utilized in the laboratory test. The seven timber deck sections (6.10 m long x 0.84 m wide x 137 mm thick) were secured to the composite superstructure at the skew angle of 12.5°, so that they were oriented parallel to the foundation beams. The decking was secured to the composite beams using a spanner design consisting of 178 or 216 mm long (depending upon the beam spacing) 2 x 4 lumber and lag bolts (159 mm diameter x 152 mm long) as shown in Figure 7. Deck-to-stringer connections in the field-constructed bridge are through-bolt connections (as shown in Figure 4). Lag bolts were used in the lab to minimize the number and depth of holes put in the deck prior to construction. The number and location of deck-to-stringer connections were varied in two different sets to assess the effect of connections on composite action. These connections were positioned according to Figure 8. The first set employed roughly one third of the number of connections made in the actual structure, while the second set utilized the full number of connections on only one lane of the bridge. No stringer-to-abutment connections were utilized, in contrast to the actual bridge design. Spanner connections (as shown in Figure 4) similar to those used for the decking are present at eight locations along the length of each abutment to secure the bridge from being laterally pushed from its foundation should flooding occur. Therefore, the composite beams were permitted to rotate and uplift at their supports. The rub rail system also was not installed for the lab testing and thus curb-stiffening was not studied in the lab test.

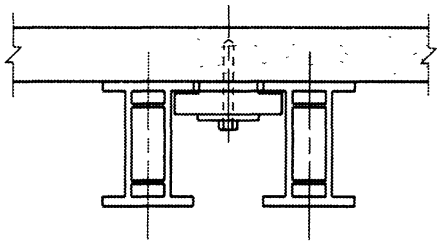

Figure 7. Schematic of beam-deck connection for lab tests.

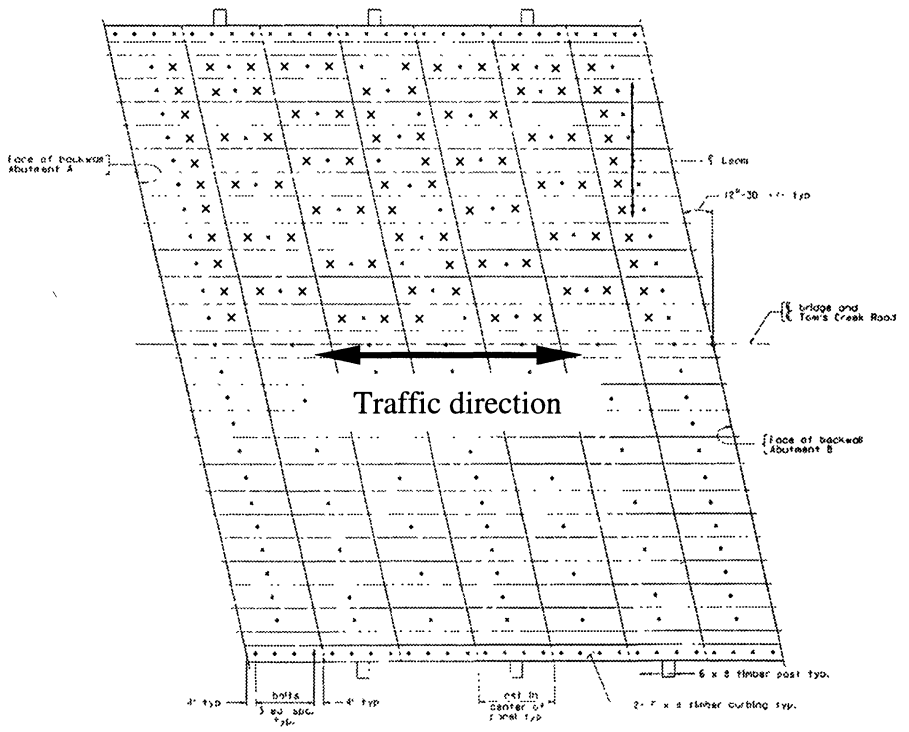

Figure 8. Two different connection sets utilized in the laboratory bridge testing. The first (single) connections are designated by dots; the additional connections (forming the second connection set) are designated by X's.

The steel load frame permitted two separate actuators to be positioned at various locations to simulate several loading scenarios. Because of the short span of this bridge, the HS20-44 design loading case occurs when one vehicle axle is positioned at mid-span near the side of the bridge (610 mm from the curb) and the other axle(s) are off the bridge. This case produces the greatest bending moment on the composite stringers. An HS20-44 axle loading of 187 kN (41.6 kip) was used in all cases; a 142 kN (32 kip) load increased by an assumed impact factor of 1.3 (as specified by AASHTO, 1996). This impact factor applies to short span steel and concrete bridge design; an appropriate impact factor for bridges containing composite girders has yet to be determined.

In the lab testing, three different types of static loading were performed (illustrated in Figure 9): Axle loads were simulated using a steel spreader beam to distribute an actuator load to the two wheel patches (508 mm long x 305 mm wide). The three loading conditions are summarized below.

- HS20-44 design loading distributed to two representative wheel patches (93.4 kN each) positioned 610 mm from the right edge at mid-span (axle orientation A).

- Two tandem HS20-44 loads (both 187 kN for a total of 374 kN), with the second axle load applied on the left side of the structure in-line with the original axle load (axle orientations A and B).

- A single HS20-44 axle load centered in the middle of the bridge (axle orientation C).

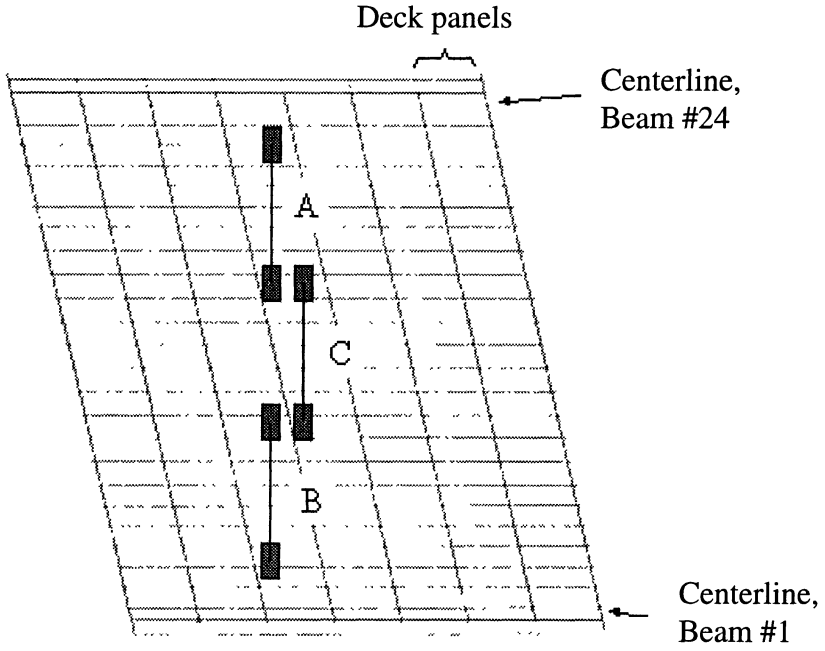

Figure 9. Loading scenarios applied for the HS20 loading tests.

Hydraulic actuators (capacities of 445 kN) and 222 kN capacity load cells were utilized to provide and record the axle loads via a wide flange spreader beam (see Figure 6). Foil strain gages were mounted at various locations to measure bending strains on the bottom flanges of the composite beams. In order to measure any composite action, strains on both the top and bottom flanges of select composite beams, as well as on the top surface of the deck were measured. Deck strains were monitored using extensometers rigidly mounted with wood screws to the middle timber deck section. These extensometers were oriented directly above and parallel to composite beams 14, 16, 18, 20, and 24. Timber deck deflections mid-way between composite girders at mid-span of the bridge were measured using wire potentiometers. In addition, the deflections at the gap between the two deck panels nearest the loading were monitored to determine the relative panel deflections. Acoustic emission was also monitored at selected sites on the composite beams. However, only a small amount of emission was expected since the predicted stringer loads under HS20-44 loading would not exceed the maximum load applied in the proof testing of the individual beams (termed the *Kaiser Effect*, Duke et al., 1998).

Field Testing

Field testing of the rehabilitated bridge was performed to establish service load deflection, strain levels, load distribution, the degree of composite action, and dynamic load effects. The first of several controlled vehicle field tests was conducted in October of 1997 by Virginia Tech and VTRC with a 214 kN (24 ton) dual rear axle VDOT truck (Figure 10). Dynamic tests were conducted with the vehicle traveling over the bridge at speeds of roughly 40 and 64 km/h (25 and 40 mph). The maximum safe speed of the test vehicle on the bridge was 64 km/h therefore this was the maximum test vehicle speed used during the field test. Quasi-static tests were also performed with the vehicle traveling at about 3 km/h (2 mph). Each test was run at three locations consistent with the loading cases investigated in the lab testing: left lane, right lane, and center of the bridge. Prior to testing, each stringer-deck connection was tightened to 41 N-m.

Figure 10. Field test of the Tom's Creek Bridge.

Field instrumentation included strain gages, Weigh-In-Motion (WIM) gages, and deflection gages along the mid-span of the bridge. Strain gages were placed at the bottom and (inside) top flanges of 12 composite girders (beams 1-5, 8-10, 12, 16, 17, 22, and 23, as referenced in Figure 11). As in the laboratory testing, gages were affixed to both the top and bottom flanges of a few FRP composite stringers to assess the amount of composite action, if any. The deflection of girders 1, 2, 4, 5, 8, 10, and 12 was also measured using cantilever deflection gages. WIM gages were used to measure the longitudinal strains on the underside of the timber deck. Five WIM gages were affixed to the deck adjacent to the instrumented girders (between composite beams 2/3, 9/10, 11/12, and 12/13).

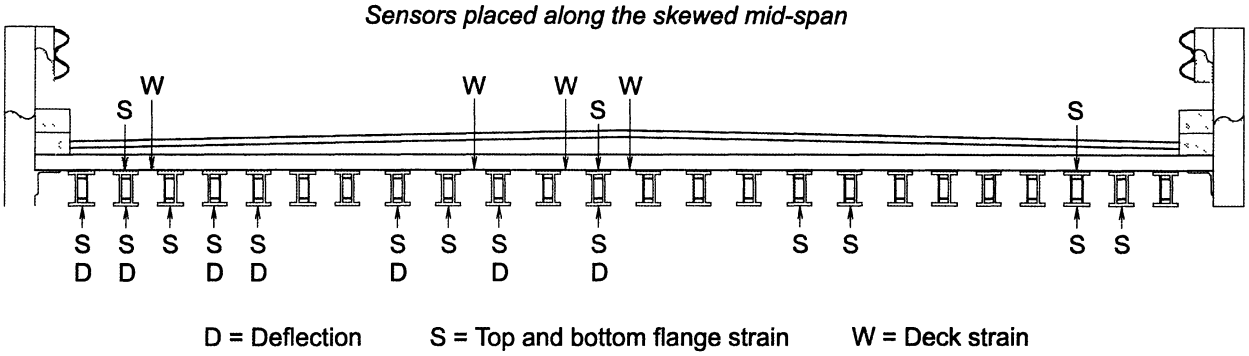

Figure 11. Locations of sensors across width of bridge for field test.

RESULTS & DISCUSSION

Laboratory Testing of Bridge Girders

Infrared Thermography

The extreme surfaces of the flanges and the outer web box each beam were examined using IRT. Few detectable variations were observed in the over 400 square feet of surface examined. The IRT method was capable of detecting subtle processing variations. For instance, a fold in the structural fabrics was imaged in the flange, as illustrated in Figure 12. Distortion of the glass stitched laminates, which make up 90% of the glass fiber in the system, by the unidirectional carbon fiber was confirmed by viewing the edge of the beam. Differences in the thermal conductivity of these materials made it possible to distinguish such fiber architecture features within the pultruded structure.

A resin-starved region of one beam was easily detected in the IRT videotape. A sequence of image associated with the imperfection is shown in Figure 13. This most severe portion of this imperfection was confirmed visually, and tapping was used to confirm that the extent of the imperfection was consistent with the associated thermal image. This beam was not used in the construction of the bridge.

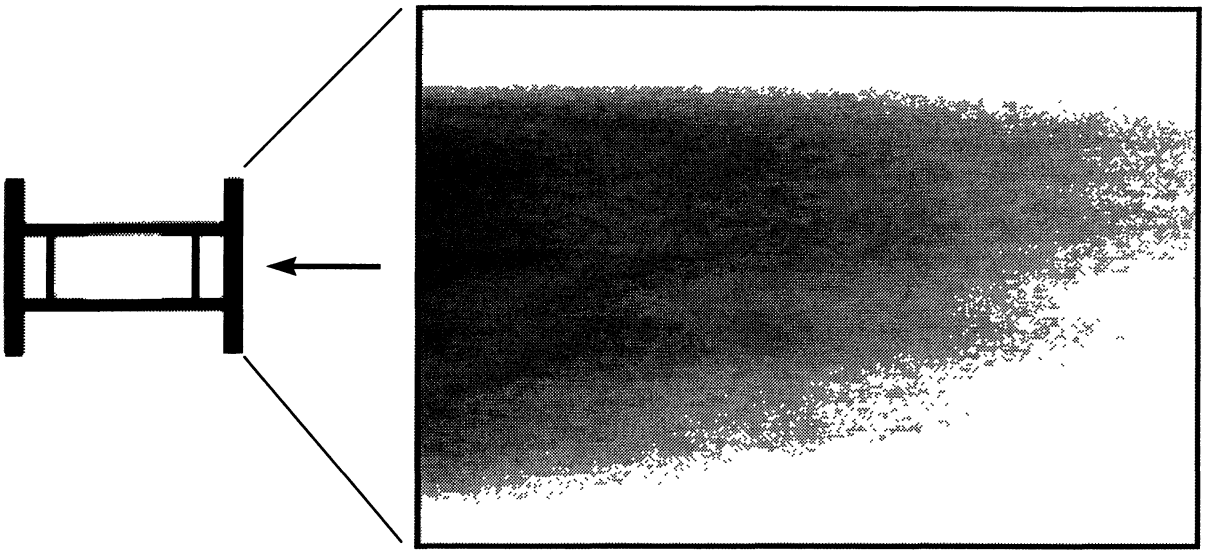

Figure 12: Infrared thermographic image (negative) where the beam is translating to the right, the temperature gradient has elevated temperature to left, and the presence of the webs are visible as lighter horizontal regions just below and above a light horizontal region apparently caused by a wrinkle in the reinforcing fiber layers.

In another beam a delamination near the end, probably induced during the cutting of the beam from the pultruded trunk was detectable, as shown in Figure 14. This sequence of images is from the videotape proceeding and at the end of the beam. The thermal gradient at the end gradually "flattens" as the end of the beam moves away from the heat lamp, allowing no additional heating of the beam. After careful examination of the IRT data and visual confirmation of the delamination this beam was excluded from use in the final bridge construction.

Acoustic Emission Monitoring

In order to provide design data to the engineer of record, one beam was loaded in four-point bending to increasingly higher deflections, with intermingled unloading, until finally the beam failed. Two plots displaying the AE detected during these loading sequences is shown in Figures 15 and 16. These data were obtained by placing one AE sensor on the bottom flange (which experiences primarily tensile loading). The AE detected on the tensile flange exhibit the Kaiser effect, (that is the AE does not reoccur upon reloading until the previous maximum load is reached) while that from the compressive flange appears to exhibit a Felicity ratio that is quite low. (The Felicity ratio was developed to generalize the Kaiser effect concept and corresponds to the ratio of the load for which AE is observed on reloading to the previous maximum loading. A material exhibiting the Kaiser effect has a Felicity ratio of 1.)

AE events were monitored during the course of proof testing for each beam installed on the bridge. Comparison of beam AE response found them to be very repeatable with no unusual responses. Upon reloading the Kaiser effect was observed in all beams, at these stress-strain levels.

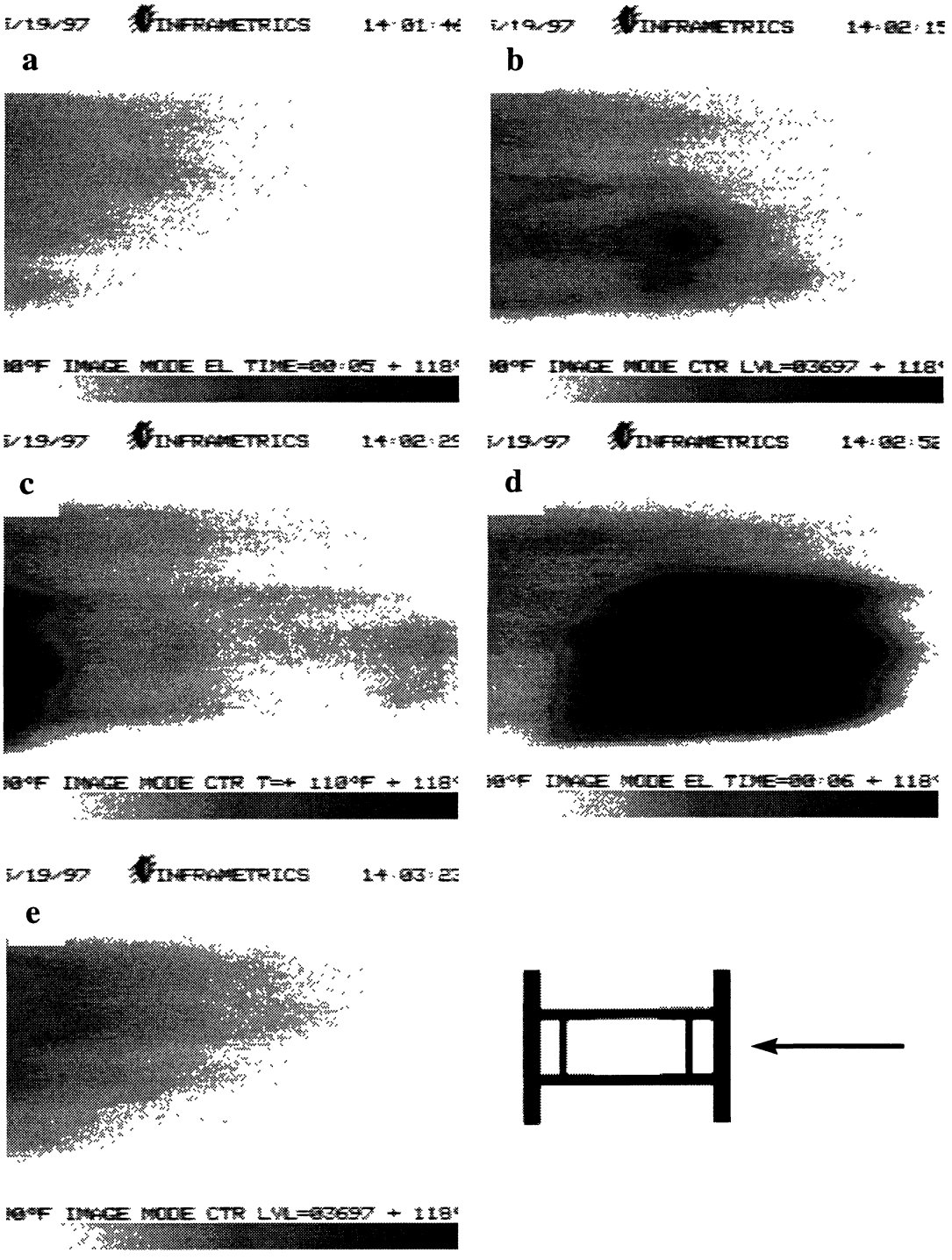

Figure 13: Sequence of IRT images (negative) where the beam is translating to the right, with a heat source irradiating the observed surface upstream (to the left). The flange surfaces are examined in this set of images. The very dark region in **frame d** (associated with a resin starved ply that is unable to dissipate the heat) enters in **frame c** and exits in **frame e** from view as the beam moves past the IRT camera.

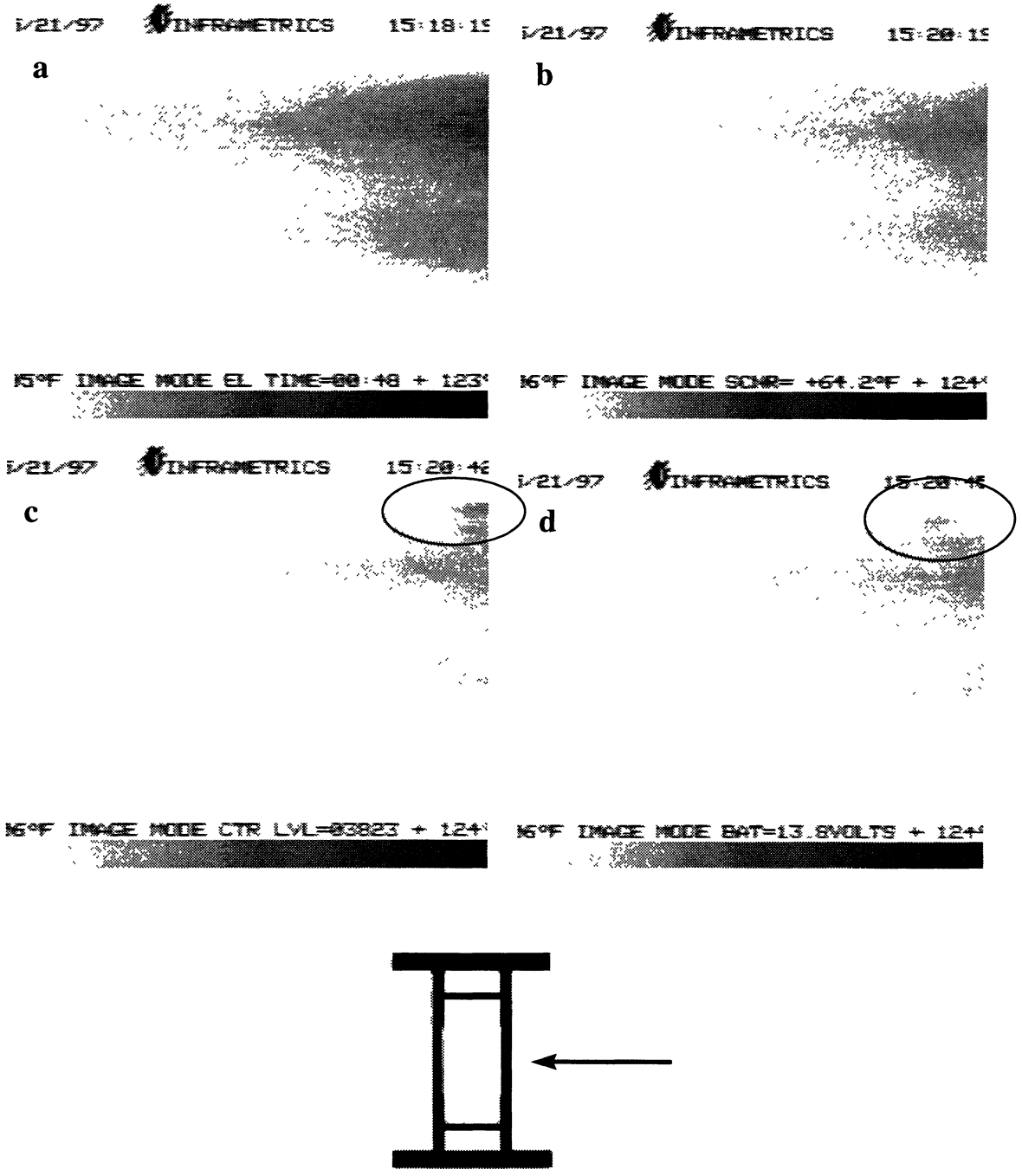

Figure 14: Sequence of IRT images (negative) where the beam is translating to the right, with a heat source irradiating the observed surface upstream (to the left). The web surfaces are examined in this set of images. In **frames c** and **d** a bump (slightly hotter region) in the thermal pattern is present at the web–flange intersection. This is caused by a delamination that limits the heat dissipation. The overall pattern lightens because the end of the beam has moved beyond the heat source, so no additional heat is added as the end of the beam moves past the IRT camera.

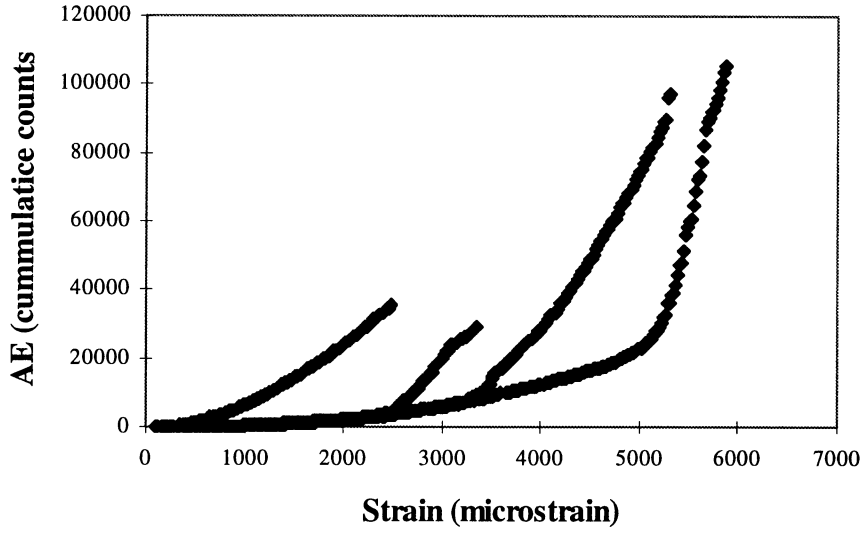

Figure 15. AE detected from a transducer placed on the **compression flange** during loading of a beam ultimately loaded until failure. The AE detected during unloading is not displayed, and AE was detected during each loading until the load increase was terminated, with some low levels of AE detected during momentary holds at maximum load.

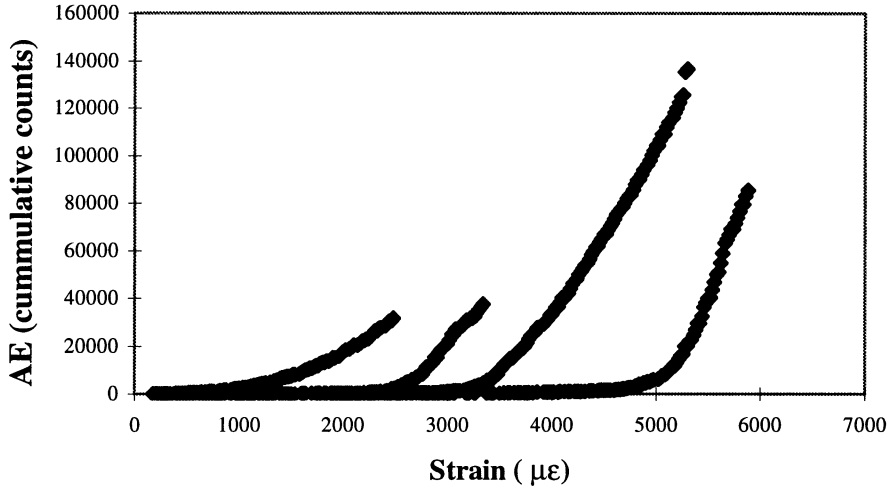

Figure 16. AE detected from a transducer placed on the **tension flange** during loading of a beam ultimately loaded until failure. The AE detected during unloading is not displayed, and AE, once detected during each loading persisted until the load increase was terminated, with some low levels of AE detected during momentary holds at maximum load.

AE was monitored during the proof test of the fully assembled bridge structure. AE sensors were placed on beams at areas predicted to be exposed to high stresses from the HS 20 testing procedure. Essentially no AE was detected during these tests, which did not cause strains in the beam to exceed those achieved during individual beam proof tests.

Acousto-Ultrasonic Evaluation

AU evaluation was performed in regions of load application during a four-point load bending cyclic fatigue test of one beam. The AU evaluation was made with and across the primary axis of the beam following an increment in number of loading cycles. Figure 17 displays an example of the AU evaluation results with and transverse to the reinforcement direction for one of the regions. The AU evaluation is essentially constant for each direction, with the difference in values between the two directions due to the decreased energy transmission across the fiber direction. Residual flexural stiffness measurements after each increment in cycles indicate that essentially no change was detected at this level of strain even after 3x 10^6 cycles.

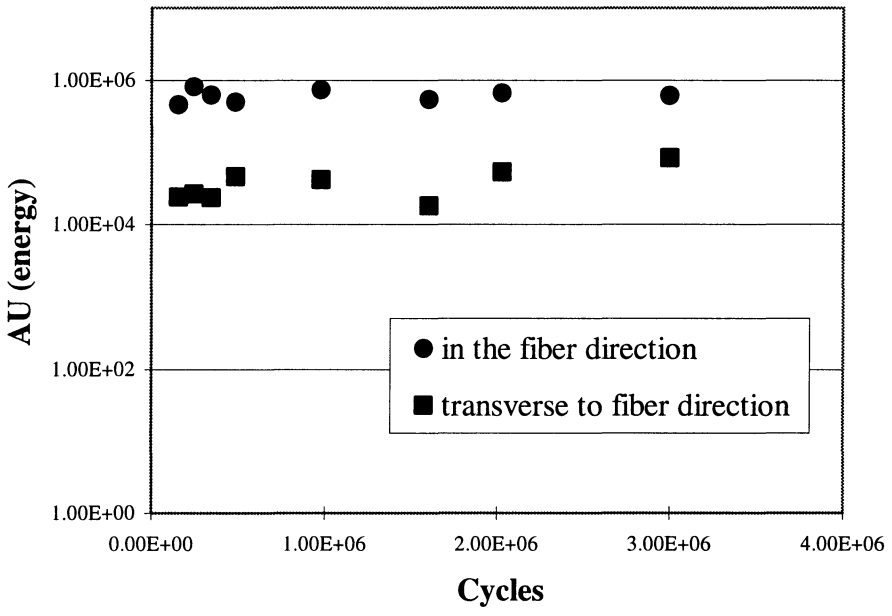

Figure 17. AU evaluation, quantified by energy detected by placing a receiving transducer in a direction with respect to the exciting transducer either in the fiber direction or transverse to the fiber direction, after different numbers of accumulated load cycles.

HS20 Loading on Side of Bridge

For the side loading scenario (loading case A in Figure 18), the wheel loads were positioned above composite beams 15/16 and 21/22, at locations of 4.27 m and 6.10 m respectively (measured with reference to beam #1, along the centerline). The largest deflection and strain values were observed at beam 22; a maximum deflection of 27 mm was measured at an axle load of 187 kN (a 72 kN wheel load with a 30% dynamic load allowance). This indicates an L/200 deflection response, L/255 if the impact factor is excluded, where L is the clear span. Again these measurements are taken from the structure which does not include curb rails and foundations connections. The maximum strain at the 187 kN axle load was 979 με. Deflections and strains for the side loading case with single connections only are shown in Figure 19 and Figure 20. The positive deflections and strains between composite beams 1 and 4 (0 to .82 m) indicate uplift at the structure's edges. Recall that the beams were not constrained at the abutments so as to prevent upward vertical displacement.

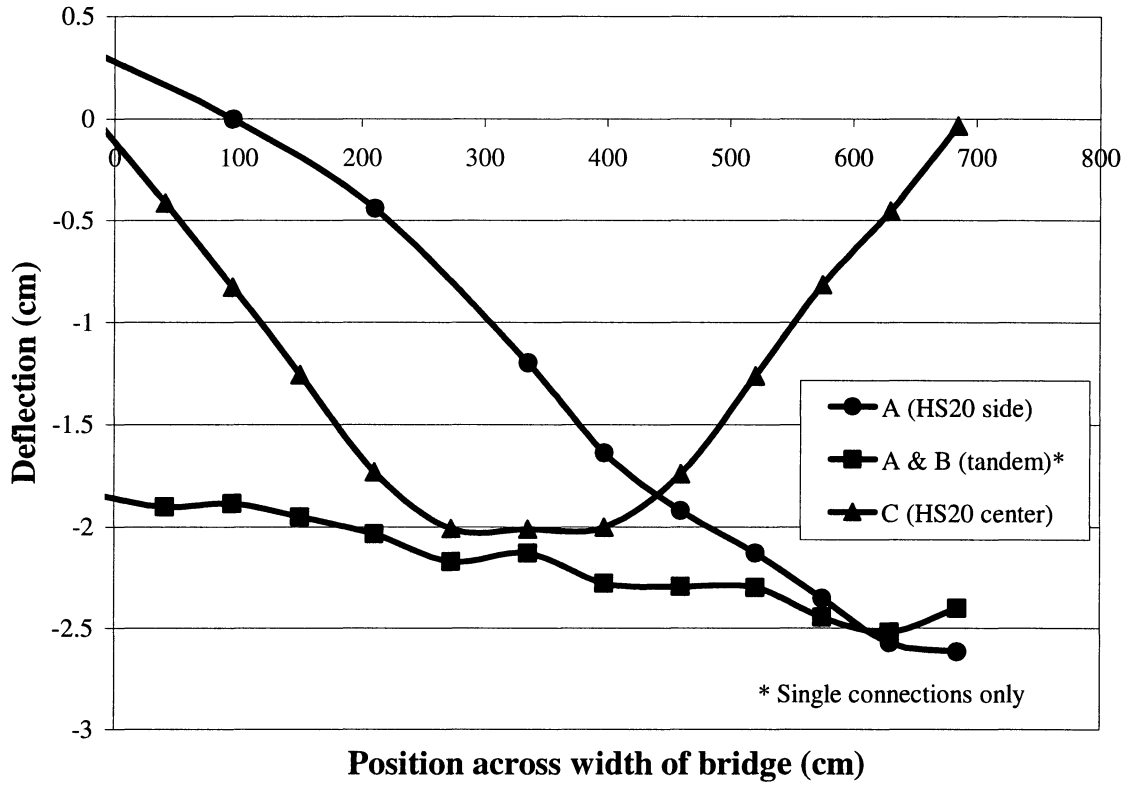

Figure 18. Comparison of deck panel deflections for three HS20 loading cases. Cases A and C are for triple connections, while the tandem loading results are for single connections only.

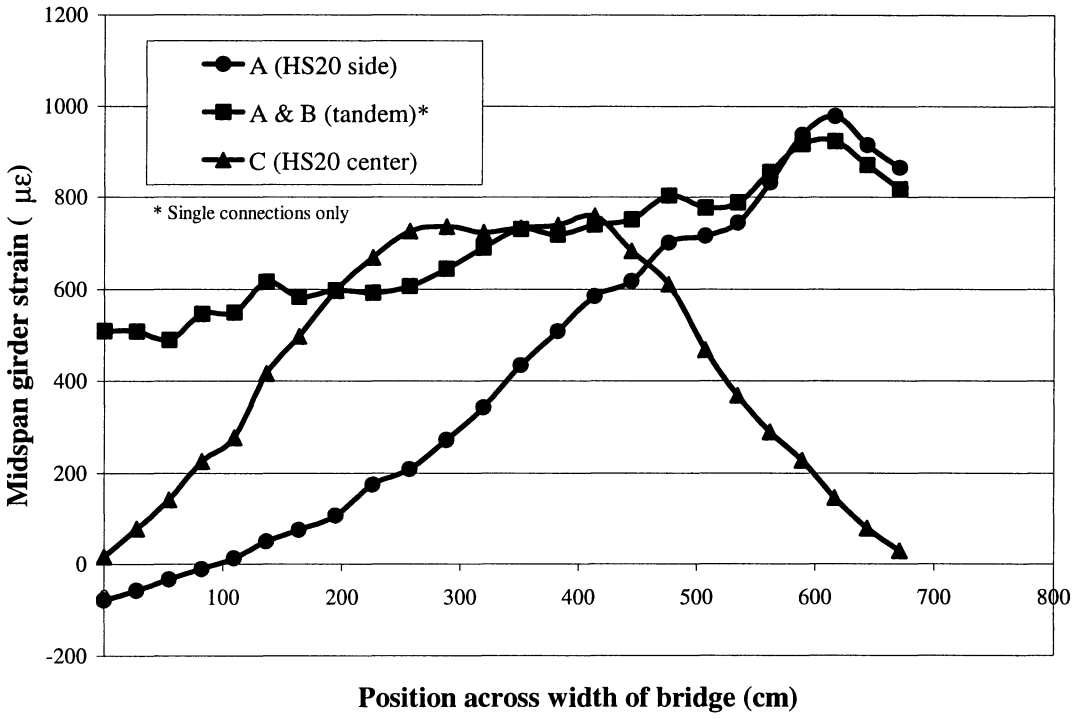

Figure 19. Comparison of center bending strains under different HS20 loading cases.

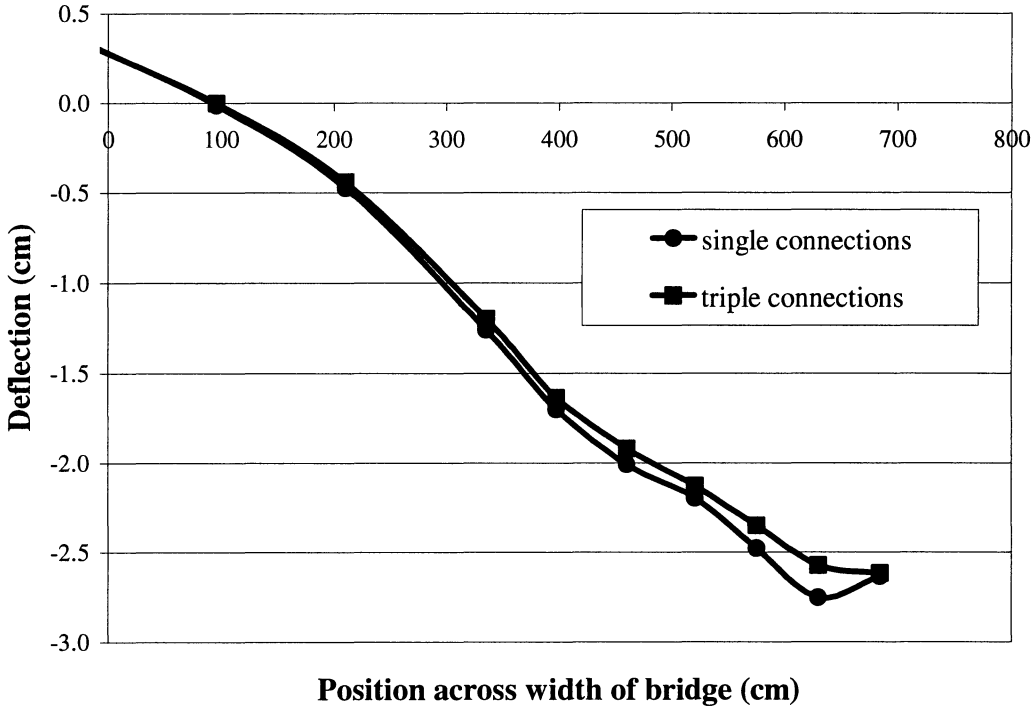

Figure 20. Mid-span deck panel deflections under HS20 side loading with two different connection sets.

Tandem HS20 Loads

Deflections and strains were measured for the tandem loading situation (loading locations A and B) to evaluate the response under two HS20 truck axle loads (see Figures 18 and 19). The wheel loading patches were positioned over composite beams 3/4 (61 cm), 9/10 (244 cm), 15/16 (427 cm), and 21/22 (610 cm). Again, only the single connection set was used. Under this loading, the maximum deflection was just under 2.5 cm, measured between composite beams 22 and 23 at a location of about 635 cm. The deflections under the B-axle wheel loads were somewhat less (1.9 to 2.2 cm), because the B-axle was located closer to one end of the composite beams as a result of the bridge's skew. The maximum strain recorded was 923 με on composite beam 22 (Figure 19). The deck strain response was nearly indentical to that observed with the HS20 side loading with a maximum tensile strain of ≈ 200 με.

HS20 Side Loading: Effect of Connections

In order to determine the effect of the connections on the degree of composite action, the additional connections were added (as illustrated in Figure 8). On the right half of the structure (nearest the loading), two more spanner connections (for a total of three) were added at nearly all of the connection sites. Thus, the number of connections on that half of the structure was nearly the same as what is being utilized in the actual bridge. The structure was then loaded under the side loading design scenario. The deflections and strains decreased only slightly (6-7%) with the additional connections (Figures 20 and 21). The timber deck strains increased some with the addition of more connections, but the maximum deck strain was still relatively small at 245 με. Furthermore, the change in the location of the neutral axis of the composite beams was negligible (less than a 2% shift), indicating little or no composite action.

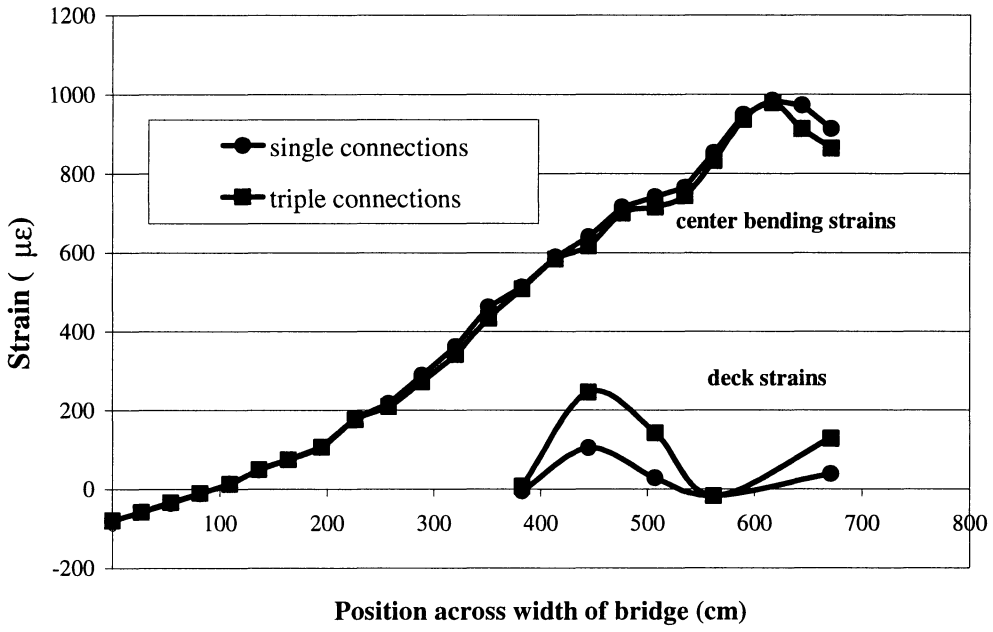

Figure 21. Girder bending and deck strains under HS20 side loading with two different connection sets.

HS20 Loading in Center of Bridge

Loading in the center of the bridge was next performed using connection set 2. The two wheel loads were located above beams 9/10 (244 cm) and 15/16 (427 cm), and the largest deflection at 187 kN was 2.0 cm (see Figure 18). The largest strain recorded was 760 με on composite beam 15 (Figure 19). Both the deflection and strain profiles were fairly symmetric. Any differences from one side of the bridge to the other may be attributed to the additional connections on the right side or variations in beam properties across the bridge.

Displacement of Foundation Beams and Inter-panel Differential Deflection

The relative motion of the deck to the abutments was a concern, as excessive relative displacement can damage the overlay. The deck panel deflections previously reported also included deflection associated with the foundation beams. Therefore, the displacement of one foundation beam on the side nearest the loads in loading case A was monitored using dial gages. The maximum displacement was approximately 0.13 cm at the edge of the top flange. Uplift at the ends of the beams were also monitored and were observed to be approximately 0.18 cm. This amount of deflection can be absorbed by the asphalt design, which incorporates a fiber reinforced rubber membrane placed between the course base and the finish grade, as noted by (Howard et al., 1997). Thus, reflective cracking under this amount of deflection should not present a problem for the long-term performance of the bridge. Again, the traffic on this structure is low, and 95% of the traffic is two-axle commuter traffic.

The inter-panel differential deflection (relative displacement between deck panels) was also measured between 1) panels 4 and 5 for the side loading (case A, with triple connections) and 2) panels 4 and 5, as well as 3 and 4, for the center loading (case C, triple connections). Of the two HS20 loading situations, the side loading was most severe; the maximum inter-panel differential deflection was 0.12cm. In this case, the two load patches were applied to two different deck panels. The work by Howard et al. indicated that a maximum inter-panel differential deflection of 0.13cm (0.05 in) could be accommodated with this particular wearing surface design (Howard, 1997). Following 22 months of service (to date), the wearing surface has not exhibited any reflective cracking and appears to be in good shape, consistent with the findings of (Howard, 1997).

Field Testing

A VDOT tandem axle dump truck loaded with gravel was used as the test vehicle during the field tests. The front and rear axle of the loaded dump truck loads was 53.4 kN and 217 kN, respectively. Typical strain vs. time profiles is shown in Figure 22 for one girder to illustrate the bridge's response to the three axle vehicle. Sample deflections measured along the center deck panel (at mid-span) are shown in Figure 23 for the side and center loading cases. The side loading deflection profile was constructed using data from test runs over both lanes of travel; deflections across only one-half of the structure were measured during the center loading runs. This data corresponds to the peak mid-span values under the 3 km/h, quasi-static front axle load (53.4 kN). The maximum deflection under this loading case was measured to be 0.38 cm, corresponding to a service load deflection of L/400 (including impact factor) when the

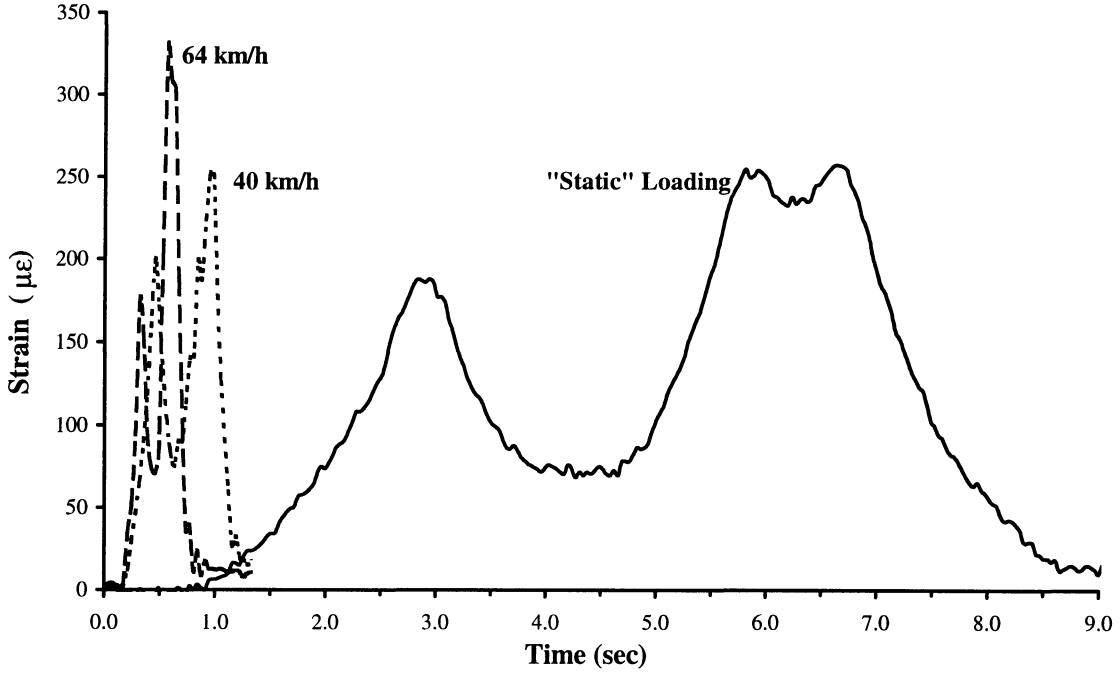

Figure 22. Dynamic response of the bridge during field tests. Maximum bending strains (girder #4) are shown for each vehicle speed.

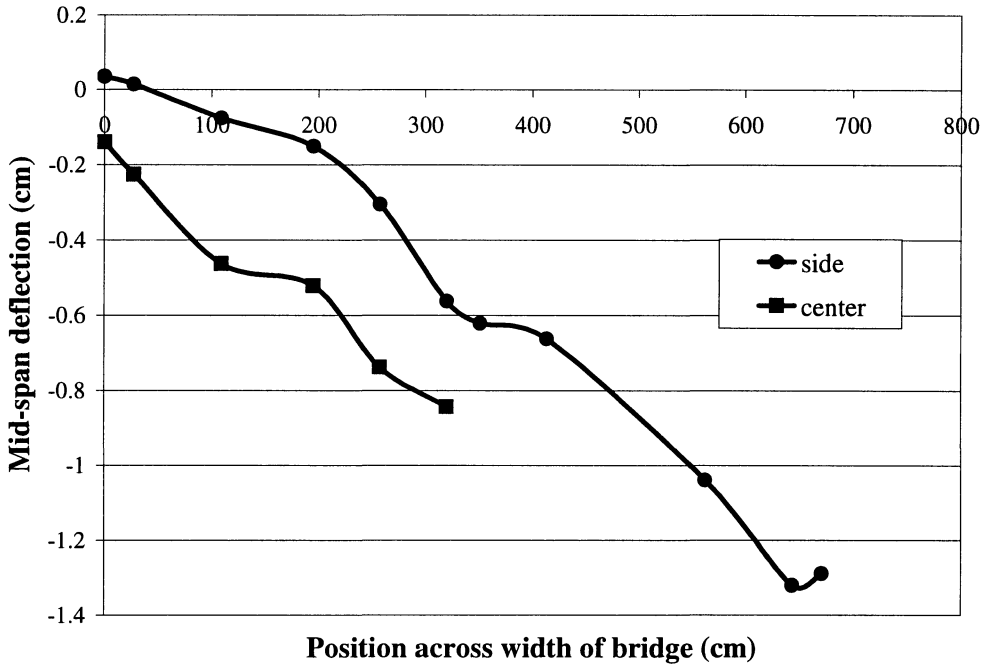

Figure 23. Center deck panel deflections under the side and center loading cases for field tests.

deflections are linearly scaled to HS20-44 loading (187 kN). This is a substantial smaller deflection as compared to the L/200 response observed in the laboratory testing, as shown in Figure 24. The increased stiffness of the field structure is due specifically to the curb stiffening introduced by the curb rails which were not present during the laboratory testing (see Figure 4). The deflection data under both side and center loading from the laboratory and field-testing are compared in Figure 24 and 25. Here again the field test data has been linearly scaled by 3.5 times to correspond to HS20-44 loading.

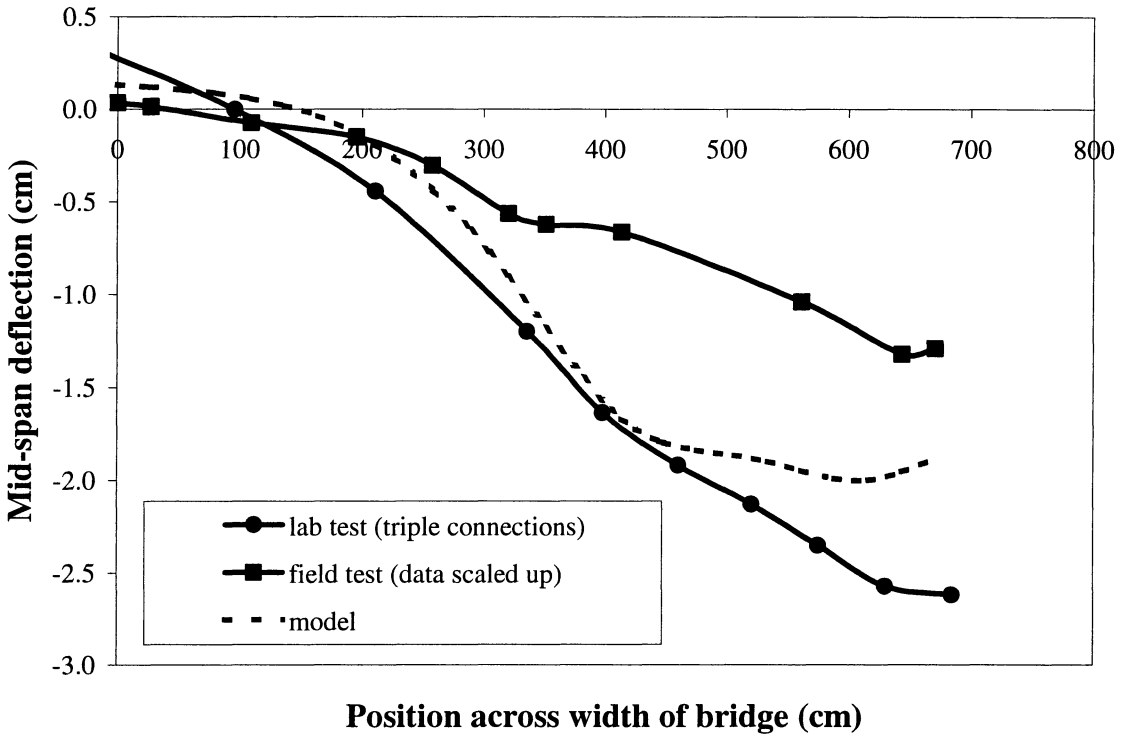

Figure 24. Comparison of center deck panel deflections under HS20-44 side loading in both the laboratory and field.

As discussed above the increased stiffness of the actual bridge as compared to the lab mock-up is most likely attributed to the addition of the rub rails along the edges of the deck. However, girder-to-abutment connections and the addition of all stringer-to-deck connections in the actual bridge can possibly contribute to the bridge stiffness.

For instance, the field test data indicated little or no uplift of the deck on the side opposite the location of the loading; i.e. the left hand side (see Figure 24). This may be attributed to the stringer-to-abutment connections, as illustrated by the deflection behavior modeled. A mechanics of materials model assumes no composite action between the stringers and the deck; i.e. the simply supported FRP beams support all of the load as distributed by the timber deck (Hayes, 1998). Uplift on the left-hand side of the bridge is lower for the model and the as constructed bridge as compared to the lab constructed bridge (see Figure 24). Thus, simply-supported end conditions are not adequate to describe the response for the lab constructed bridge

and therefore exhibit greater uplift. Moreover, these abutment connections appear to play a role in the performance of the placed bridge.

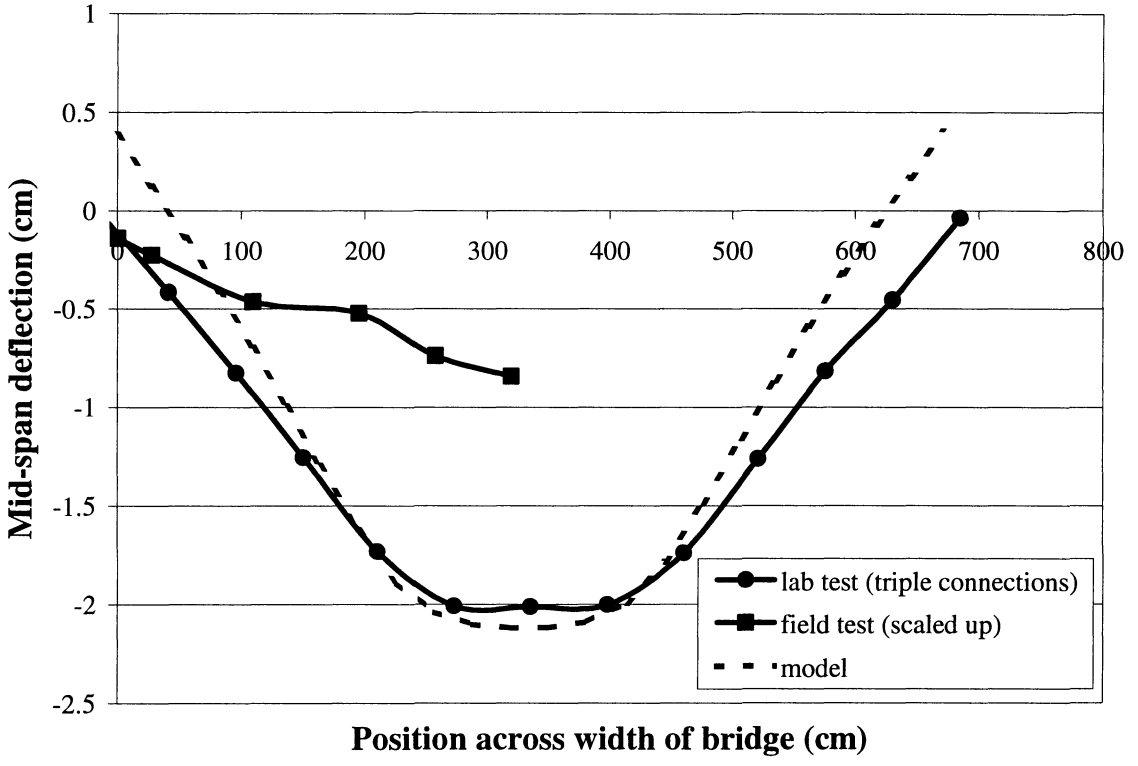

Figure 25. Comparison of center deck panel deflections under HS20-44 center loading in both the laboratory and field.

Greater stiffness of the rehabilitated bridge relative to the lab mock-up is also observed for the center loading case (Figure 25). The mid-span bending strains on the composite girders under center loading are shown in Figure 26. A maximum strain of 135 με was measured, so that under HS20-44 loading, the maximum expected strain would be about 470 με. This corresponds to a factor of safety of over 7 using the projected A-allowable for this particular span. Again, the deck strains observed during the field tests were relatively small (≈300 με) yet the shift in neutral axis was slightly greater (less than 10 %). A subsequent field test demonstrated that axial (tensile) load was present in the beams as a result of axial constraints present by the abutments (further details to be reported Rux, 1999).

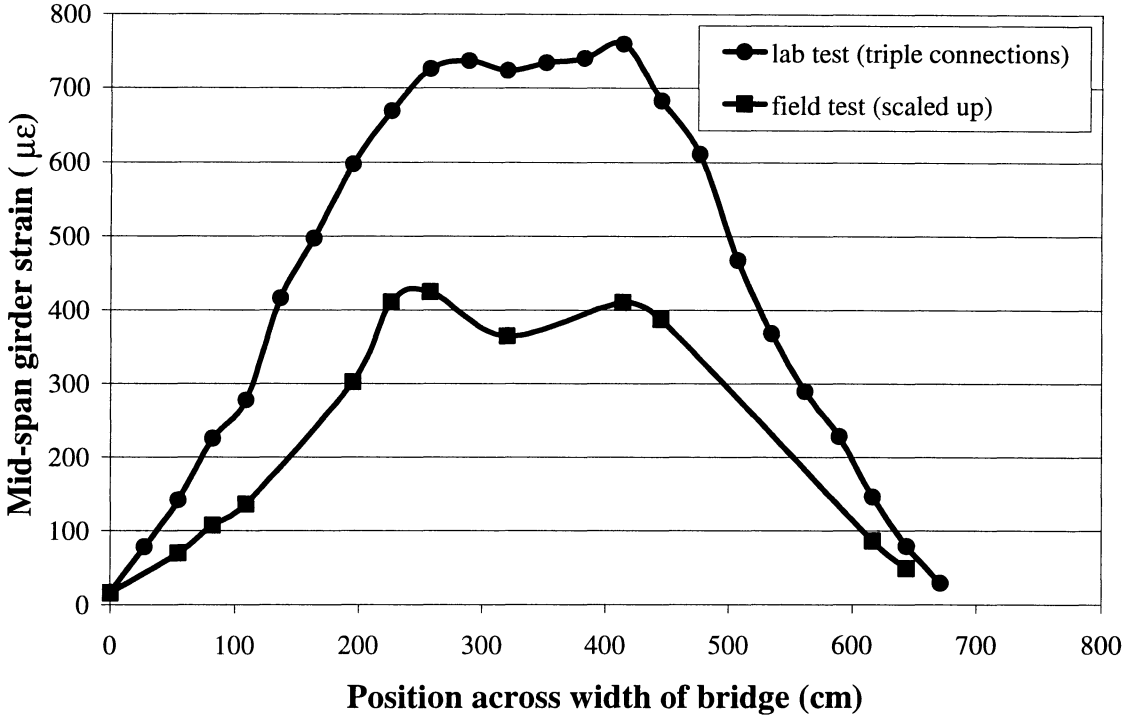

Figure 26. Mid-span bending strains on selected composite girders in field tests.

Data taken from the tests at all three speeds (3, 40, and 64 km/h) were analyzed to identify the actual impact factor for this structure. Typically, the largest increases in deflections and strain at the 64 km/h speed were, on average, 45% for center left and right lane passes, as shown in Figure 22. At 40 km/h there was a negligible dynamic effect for center left and right passes.

It is generally accepted that the analysis of the impact factor is complicated by a number of variables. First, the load distribution (and therefore maximum deflections) is likely to be very dependent on the lateral locations of the wheels (Hayes, 1998). Secondly, the dynamic loads applied by the truck may be dependent upon specific vehicle characteristics such as suspension, geometry, approach conditions and weight distribution. A more reasonable approach to identifying the dynamic characteristics may be to characterize and understand the natural frequency and damping characteristics of both the composite beam and the total bridge structure. A preliminary analysis of the bridge response to dynamic loading shows an average mid span damped natural frequency (very close to the natural frequency with the damping factor very low $\zeta \approx 0.1$) of about 14 Hz. Log decrement was used to assess this value from 118 strain and deflections measurements made across the width of the bridge for vehicle speeds of 40 and 64 km/h. This recorded damped natural frequency is roughly 18% lower than that predicted by Paultre et al. (Paultre 1992); predicted value of 16-18 Hz from $f = 82\ L^{-0.9}$ where L ranges from 6.2 to 5.3 m. This empirical expression is derived from conventional structures and is not a completely accurate comparison when considering the differences in materials and design. Yet,

a "lower" natural frequency relative to the prediction may be indicative of the lower stiffness of the structure.

Distribution of load transversely across the bridge is another design consideration. AASHTO (1996) specifies limits for load distribution on stringers for various bridge designs, but no such standard exists for bridge designs utilizing FRP composite beams. To evaluate the load distribution of the Tom's Creek Bridge superstructure, data from both the laboratory and field tests were analyzed. Bottom flange strains obtained from the following loading configurations were used for evaluating the load distribution of the Tom's Creek Bridge:

1. laboratory tests axle alignments A and B from Figure 9 were used
2. field tests truck crossings in each lane were combined.

The bending strains on the bottom flange of each composite beam were used, assuming that strains are linearly proportional to the applied load and inversely proportional to the beam stiffness in bending and shear. The percentage of load carried by each stringer was determined for the case of tandem axle loads positioned in-line at mid-span by dividing the strain on a beam by the total strains resulting from the tandem axle loads (Figure 27). The data indicates that the load distribution is fairly uniform, with an average applied load per beam of 4.2% and is independent of vehicle speed.

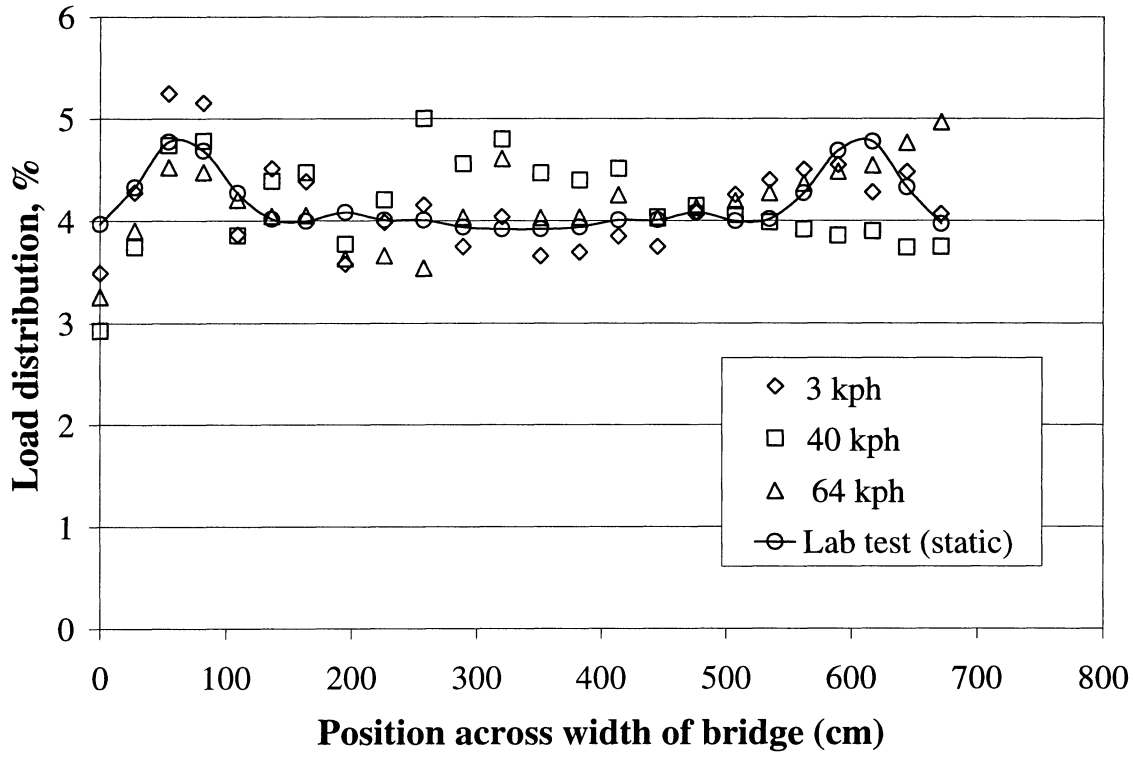

Figure 27. Load distribution across width of bridge for various field tests (dynamic and quasi-static) and lab test (quasi-static).

In AASHTO (1996), the nearest type of structure for which specifications regarding load distribution are given is a steel stringer and timber deck design. For a deck depth equal to 10.2 cm (4 in), the load fraction per beam under one wheel line loading (one wheel patch, for this bridge) is the stringer spacing (S, in feet) divided by 4.0; Load Distribution Factor (LDF = s/4). For a depth greater than 15.2 cm (6 in), a fraction of S / 4.5 is specified. For the 13.0 cm (5.13 in) depth of the glue-lam system used here, S / 4.0 is considered for comparison purposes. The load fraction per beam under two tandem truck axles (four lines of wheel loads) would be S / 16. This corresponds to a design distribution factor of about 6% for the average girder spacing in the Tom's Creek Bridge. Therefore, in comparison with a steel/timber design, the design load distribution factor conservatively estimates the load distributed to any one composite girder.

CONCLUSIONS

Laboratory and field testing of the structure show that composite action between the timber deck and the pultruded FRP composite structural shapes is minimal for the concrete abutment, FRP stringer, and timber deck design. Although connectivity between the deck and stringers was not anticipated with the deck-to-stringer connections employed, other features in the design contribute to the structural stiffness. Curb stiffening and beam end constraints provide additional stiffness (100% stiffer) to the as constructed bridge when compared to the experiments conducted in the laboratory. The field-constructed bridge possesses a L/400 serviceability at the HS20-44 loading where lane (left or right) loading is the design load case. Maximum strains in the FRP stringers are as high as 0.01% and 0.004% for lane loading (right or left) for the laboratory and field structures respectively. This yields a considerable factor of safety where the bending $\varepsilon_{ult} = 0.6\%$. Again, strains in the deck are low ($\approx$300 $\mu\varepsilon$) as a direct result of inadequate connectivity between the deck and the stingers. Reducing the number of connections as observed in the laboratory bridge tests does not significantly affect composite action.

Although bridge design standards do not exist for this particular FRP rehabilitation, load distribution factor of span divided by 4 (LDF = s/4) is conservative in describing load fraction in each beam. This does not appear to be affected by vehicle speed. Yet the load amplification factor does appear to be a nonlinear function of speed and does not meet with the AASHTO (1996) recommendation for IM = 1.3 times the static design load. The damped natural frequency of the field-rehabilitated bridge is 14 Hz, lower than that predicted by Kim (1997).

FUTURE RESEARCH AND RECOMMENDATIONS

A series of additional field tests are planned throughout the life of the Tom's Creek Bridge. These periodic tests will be part of a larger effort to characterize the durability of the composite beams over the life of this structure. The goal of the study is to track changes in beam properties with time due to loading and environmental aging. Enviro-mechanical aging of the beams will also be assessed by periodically removing and replacing the outer two beams on the upstream side of the bridge. These beams will be evaluated using both NDE (infrared thermography) and

mechanical methods (static testing to failure). Any change in the response of the bridge, in terms of stiffness, load distribution, or impact factor, may provide an indication of material degradation as well.

ACKNOWLEDGMENTS

The authors wish to acknowledge the following for their cooperation and support in the form of material donations, financial resources, and engineering expertise: Dan Witcher, Glen Barefoot, and Clint Smith of Strongwell Inc.; Julius Volgyi, Ernesto Villalba, and Mal Kerley at the Virginia Department of Transportation; Wally McKeel and the Virginia Transportation Research Council; Jim Stewart and the Center for Innovative Technology; Randy Formica, Adele Schirmer, and the Town of Blacksburg; and Dr. Jim McGrath and the National Science Foundation Science and Technology Center for High Performance Polymeric Adhesives and Composites at Virginia Tech.

REFERENCES

Chajes, M., Gillespie, J., Mertz, D., and Shenton, H. (1998). Advanced Composite Bridges in Delaware. *Proceedings of the Second International Conference on Composites in Infrastructure*, Tucson, Arizona, v1, 645-650.

Composite Structural Shapes for Infrastructure. (1994). National Institute of Standards and Testing Advanced Technology Program, Morrison Molded Fiberglass.

Duke, J.C., Horne, M.R., and Johnson, A. (1998). Baseline NDE of Pultruded Composite Bridge Beams. *Proceedings of the Second International Conference on Composites in Infrastructure*, Tucson, Arizona, v2, 582-590.

Hayes, M.D. (1998). Characterization and Modeling of a FRP Hybrid Structural Beam and Bridge Structure for Use in the Tom's Creek Bridge Rehabilitation Project. *M.S. Thesis*, Virginia Polytechnic Institute and State University.

Howard, J.N. (1997). Investigation of the Structural Behavior of Asphalt/Wood Deck Systems for Girder Bridges. *M.S. Thesis*, Virginia Polytechnic Institute and State University.

Hayes, M.D., Lesko, J.J., Haramis, J., Cousins, T.E., Gomez, J., Massarelli, P. (2000), Laboratory & Field Characterization of the Tom's Creek Bridge Composite Superstructure, in press *ASCE, Journal of Composites for Construction.*

Lopez-Anido, R., Gangarao, H.V.S., Troutman, D., and Williams, D. (1998). Design and Construction of Short-Span Bridges with Modular FRP Composite Deck. *Proceedings of the Second International Conference on Composites in Infrastructure*, Tucson, Arizona, v1, 705-714.

Paultre P., Chaallal, O., and Proulx, J., (1992). Bridge dynamics and dynamic amplification factor – a review of analytical and experimental findings. *Canadian J. Civil Engr.,* **19**, pp. 260-278.

Plunkett, J.D. (1997). Fiber-Reinforced Polymer Honeycomb Short Span Bridge for Rapid Installation. *IDEA Project Final Report*, Contract NCHRP-96-ID030, Transportation Research Board, National Research Council.

Proposed Bridge on Tom's Creek Road Over Tom's Creek Bridge, Town of Blacksburg. Tom's Creek Bridge design plans. Commonwealth of Virginia Department of Transportation, May 8, 1997.

Richards, D. (1997). Lockheed Corporation – Bridge Design. Presentation at the Midwestern Workshop for Fiber Reinforced Composite Infrastructure, Hamilton, Ohio, August 27, 1997.

Richards, D., Dumlao, C., Henderson, M., and Foster, D. (1998). Methods of Installation and the Structural Analysis of Two Short Span Composite Highway Bridges. *Proceedings of 1998 International Composite Expo*, Nashville, TN, Session 4-E, 1-6.

Rux, K., Cousins, T.E., and J.J. Lesko, (1999). Load Testing and Structural Performance of the Tom's Creek Bridge. *To be submitted to Journal of Composite for Construction.*

Strongwell, Corp., (1995). NIST Advanced Technology Program. Development of Innovative Manufacturing Technology to Produce a Large Phenolic Composite Shapes.

Standard Specifications for Highway Bridges. (1996). American Association of State Highway and Transportation Officials, Washington D.C.